COMPUTATIONAL MODELING OF PARTICLE DEPOSITION PROCESSES

Eduardo M. B. Campello

campello@usp.br

Department of Structural and Geotechnical Engineering

Polytechnic School, University of São Paulo

P.O. Box 61548, 05424-970, São Paulo, SP, Brazil

Abstract*. This work presents a computational model for the simulation of industrial particle deposition processes. The approach is based on the discrete element method (DEM), whereby the deposition material is treated as a discrete medium that is targeted at a base substrate with varying process parameters. We use phenomenological models to describe the various forces involved at the level of the particle interactions. Particular attention is devoted to the modeling of particle contact and adhesion, since inter-particle bonding and agglomeration are crucial aspects in any such deposition methods. Examples of numerical simulations are shown to illustrate the potentialities of the scheme. We believe that consistent DEM models may be a useful tool for the simulation of many modern particle deposition processes, such as (but not limited to) additive manufacturing techniques, 3D printing methods, deposition of thermal and mechanical barrier coatings onto surfaces, thin films, and many others wherein matter is additively placed into shape.*

Keywords: *particles; particle deposition; discrete element method; additive manufacturing, 3D printing.*

1 INTRODUCTION

Particle deposition is a widely used technique in many industrial processes. In the manufacturing industry, in particular, it is in the core of nearly all modern methods of fabrication of objects, as well as in a myriad of surface engineering processes. Most of these methods may be collectively grouped into the class of so-called additive manufacturing methods, in the sense that they are processes whereby objects are fabricated or engineered by additively placing material (originally in the form of solid particles) in a layer-wise fashion under computer control, often with some source of heating, until a desired form or three-dimensional shape is attained. One particular type of additive manufacturing methods are the so-called material jetting methods. Material jetting creates objects by depositing droplets or jets of fine particles (typically of some metal or polymeric material) from a nozzle onto a build platform. The nozzle moves horizontally and vertically, whereas the platform stands still. The particles adhere to each other upon impact with the platform (usually with no use of external heating) and form a layer of bulk material. The deposition is repeated in a layer-upon-layer way, until the desired shape is complete. Depending on the application, the layers may be cured or hardened by UV light after deposition. This work presents a computational model for the simulation of these types of deposition processes. Our approach is based on the discrete element method (DEM), such that the deposition material is treated as a discrete medium that is targeted at a rigid substrate with varying process parameters (impact velocity, elastic properties, particle size distribution, etc.). We follow a purely mechanistic description and use phenomenological models to represent the various forces involved at the level of the particle interactions. Particular attention is devoted to the modeling of particle contact (including stick-slip friction and rolling resistance) and adhesion, since inter-particle bonding and agglomeration are crucial aspects in any such deposition methods. A time-stepping integration scheme is developed for solution of the system´s dynamics, and examples of numerical simulations are provided to illustrate the potentialities of the scheme. We believe that consistent DEM models may be a useful tool for the simulation of many modern particle deposition processes, such as (but not limited to) additive manufacturing techniques, 3D printing methods, deposition of thermal and mechanical barrier coatings onto surfaces, thin films, and many others wherein matter is additively placed into shape.

The paper is organized as follows. In Section 2 we describe our DEM formulation, including detailed representations of the several forces involved. In Section 3 we present the time integration scheme that we adopt for the solution of the system's dynamics, including an algorithmic overview. In Section 4 we show three examples of numerical simulations to illustrate the applicability of our scheme, and in Section 5 we close the paper with some final considerations. Throughout the text, plain italic letters ($a, b, \ldots, \alpha, \beta, \ldots, A, B, \ldots$) denote scalar quantities, boldface italic lowercase letters ($\boldsymbol{a}, \boldsymbol{b}, \ldots, \boldsymbol{\alpha}, \boldsymbol{\beta}, \ldots$) denote vectors and boldface italic capital letters ($\boldsymbol{A}, \boldsymbol{B}, \ldots$) denote second-order tensors in a three-dimensional Euclidean space. The (standard) inner product of two vectors is denoted by $\boldsymbol{u} \cdot \boldsymbol{v}$, and the norm of a vector by $\|\boldsymbol{u}\| = \sqrt{\boldsymbol{u} \cdot \boldsymbol{u}}$.

2 DEM FORMULATION

The DEM model presented in this section follows the approach proposed by the author in Campello (2015a, 2016, 2017). Accordingly, collections of particles are treated as discrete dynamical systems following a purely mechanistic description, wherein each particle interacts

with the others and the surrounding medium via a combination of various different forces. These are external field forces (from gravity, electric and/or magnetic exterior fields), drag forces (from surrounding fluids), near-field forces (attractive and repulsive interactions), adhesion forces (from occasional bonding), and contact and friction forces due to touching and collisions. Although these forces may (and, in the general case, do) act in the particles at the same time, the last three are certainly the dominant forces here, once we are concerned with particle deposition processes in this work. Classical dynamics is adopted to describe the time evolution of the systems, the equations of which are solved via a numerical (time-stepping) integration scheme. The particles have both translational and rotational motions (in this sense, the model presented in this section may be seen as a generalization of the models presented previously by Campello and Zohdi (2014a, 2014b) and Campello (2015b), wherein rotations and spins were not considered). For the sake of simplicity, but without any loss of generality, we consider here only spherical particles.

3.1 Equations of motion

Let the system be comprised of N_P particles, each one with mass m_i, radius r_i and electric charge q_i ($i = 1,...,N_P$). Let the center of a particle be designated by C_i, and the particle´s rotational inertia relative to it by $j_i = (2/5)m_i r_i^2$. Let $\{\mathrm{O}, \boldsymbol{e}_1, \boldsymbol{e}_2, \boldsymbol{e}_3\}$ be a global (fixed) reference system, with origin at point O, and let $\{\mathrm{C}_i, \boldsymbol{e}_{1,i}^{\ell}, \boldsymbol{e}_{2,i}^{\ell}, \boldsymbol{e}_{3,i}^{\ell}\}$ be the local (body-fixed) reference system of particle i, with origin at the particle´s center. We denote the position vector of a particle by $\boldsymbol{x}_i$, the velocity vector by $\boldsymbol{v}_i$ and the spin vector by $\boldsymbol{\omega}_i$, as depicted in Fig. 1. The rotation vector of a particle relative to the beginning of the motion, which furnishes the spatial orientation of the particle with respect to the initial configuration, is denoted by $\boldsymbol{\alpha}_i$, whereas the incremental rotation vector (i.e., rotation vector relative to two consecutive configurations) is denoted by $\boldsymbol{\alpha}_i^{\Delta}$. The rotational motion between two consecutive configurations is described by the incremental rotation tensor $\boldsymbol{Q}_i^{\Delta}$, which is a function of $\boldsymbol{\alpha}_i^{\Delta}$ and is given by the Euler-Rodrigues formula

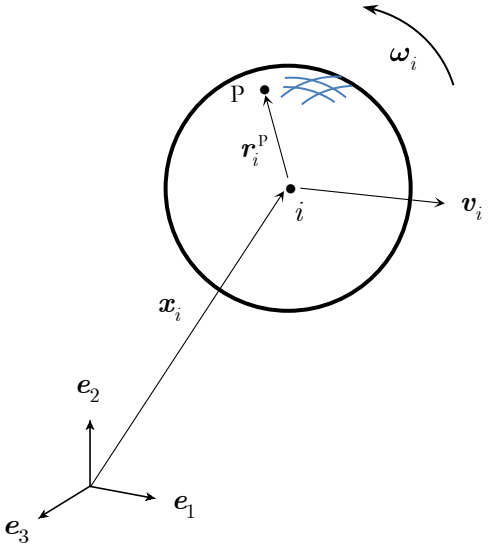

Fig. 1 Description of a single particle. Point P is on the particle's surface and may represent, e.g., the point of contact with another particle or object

$$\boldsymbol{Q}_i^{\Delta} = \boldsymbol{I} + \frac{4}{4 + \boldsymbol{\alpha}_i^{\Delta} \cdot \boldsymbol{\alpha}_i^{\Delta}} \left[\boldsymbol{A}_i^{\Delta} + \frac{1}{2} \boldsymbol{A}_i^{\Delta} \right], \tag{1}$$

wherein $\boldsymbol{A}_i^{\Delta} = \mathrm{Skew}(\boldsymbol{\alpha}_i^{\Delta})$ is the skew-symmetric tensor whose axial vector is $\boldsymbol{\alpha}_i^{\Delta}$. One should notice that the above expression referrers to a Rodrigues´ parameterization of the rotation tensor, instead of the usual one based on the Euler rotation vector. This implies that $\boldsymbol{\alpha}_i^{\Delta}$ is a Rodrigues rotation vector. We refer the reader to Campello (2015) and Campello et al. (2011) for details. One should notice also that, though the particles are assumed to be spherical, the description of their rotations is relevant to their motion, since inter-particle friction may induce rolling and thereby any material point P on the particle's surface (e.g., the contact point with another particle or object) may displace between two consecutive configurations – a motion that involves rotation and needs to be mapped if one is interested in properly capturing stick-slip and rolling phenomena. This issue will become clearer in forthcoming equations. In Fig. 1, vector $\boldsymbol{r}_i^{\mathrm{P}}$ is the vector that locates a material point P on the surface of the particle with respect to the particle´s center.

Let us denote the total force vector acting on particle i by $\boldsymbol{f}_i^{tot}$ and the total moment (with respect to the particle´s center) by $\boldsymbol{m}_i^{tot}$. According to the Euler´s laws, at every time instant t the following equations must hold for each particle:

$$\begin{aligned} m_i \ddot{\boldsymbol{x}}_i &= \boldsymbol{f}_i^{tot}, \\ j_i \dot{\boldsymbol{\omega}}_i &= \boldsymbol{m}_i^{tot}, \end{aligned} \tag{2}$$

where the superposed dot denotes differentiation with respect to time. The total force vector is made up of several force contributions as follows

$$\boldsymbol{f}_i^{tot} = \boldsymbol{f}_i^{ef} + \boldsymbol{f}_i^{drag} + \boldsymbol{f}_i^{nf} + \boldsymbol{f}_i^{con} + \boldsymbol{f}_i^{fric} + \boldsymbol{f}_i^{adh}, \tag{3}$$

in which $\boldsymbol{f}_i^{ef}$ are the forces due to external fields (gravity, electric and/or magnetic exterior fields), $\boldsymbol{f}_i^{drag}$ is the drag force vector (standing for viscous effects induced by the surrounding medium on the motion of the particle), $\boldsymbol{f}_i^{nf}$ are the forces due to near-field interactions with other particles, $\boldsymbol{f}_i^{con}$ are the forces due to mechanical contacts (or collisions) with other particles and/or obstacles, $\boldsymbol{f}_i^{fric}$ are the forces due to friction that arise from these contacts or collisions, and $\boldsymbol{f}_i^{adh}$ are the forces due to adhesion that may arise from these contacts or collisions. The total moment vector, in turn, has contributions only from the friction forces and rolling resistance effects, such that

$$\boldsymbol{m}_i^{tot} = \boldsymbol{m}_i^{fric} + \boldsymbol{m}_i^{rol}. \tag{4}$$

This implies that all forces (except for friction and rolling resistance effects) are assumed to be central effects, i.e., they act with no eccentricity relatively to the center of the particle. Each one of the force and moment contributions above is briefly described in the subsections that follow. For more details, we refer the reader to Campello (2016).

3.2 External fields force

External fields are defined here by a gravity acceleration vector $\boldsymbol{g}$, an electric field vector $\boldsymbol{E}$ and a magnetic field vector $\boldsymbol{B}$, acting on the system. These fields are assumed to be fully uncoupled and static, in the sense that they are not affected by the motion of the particles. The

forces they induce on particle i are given by

$$\boldsymbol{f}_i^{ef} = m_i \boldsymbol{g} + q_i \boldsymbol{E} + q_i \boldsymbol{v}_i \times \boldsymbol{B} \,. \tag{5}$$

The sum of the two last terms in (5) is the so-called Lorentz force. We remark that the influence of auto-induced electromagnetic fields (i.e., those generated by the particles themselves) is considered negligible, since the particles are expected to experience translational velocities that are way below the speed of light.

3.3 Drag force

The drag force has origins in the friction and pressure that the surrounding medium exerts on a particle. It is given here by the standard drag equation

$$\boldsymbol{f}_i^{drag} = -\frac{1}{2} \rho_F C_D A_i \| \boldsymbol{v}_i - \boldsymbol{v}_F \| (\boldsymbol{v}_i - \boldsymbol{v}_F) \,, \tag{6}$$

where ρ_F is the mass-density of the fluid, C_D is the drag coefficient, $A_i = \pi r_i^2$ is the "frontal" area of the particle with respect to the flow, and $\boldsymbol{v}_F$ is the (local) velocity of the fluid. The drag coefficient is assumed here to be a function of the Reynolds number of the flow, according to the model by Biringen and Chow (2011) as follows

$$\begin{aligned}
&\text{For} \;\; 0 < \mathrm{Re} \leq 1, \quad C_D = 24(\mathrm{Re})^{-1}; \\
&\text{For} \;\; 1 < \mathrm{Re} \leq 400, \quad C_D = 24(\mathrm{Re})^{-0.646}; \\
&\text{For} \;\; 400 < \mathrm{Re} \leq 3\times 10^5, \quad C_D = 0.5; \\
&\text{For} \;\; 3\times 10^5 < \mathrm{Re} \leq 2\times 10^6, \quad C_D = 0.000366(\mathrm{Re})^{0.4275}; \\
&\text{For} \;\; \mathrm{Re} > 2\times 10^6, \quad C_D = 0.18,
\end{aligned} \tag{7}$$

where Re is given by

$$\mathrm{Re} = \frac{2 r_i \rho_F \| \boldsymbol{v}_i - \boldsymbol{v}_F \|}{\eta_F}, \tag{8}$$

with η_F as the viscosity of the fluid. The assumption of C_D being dependent on Re is valid for incompressible fluids, which is the case here (in other words, we assume that the relative velocity between the fluid and the particles is below the speed of sound in the fluid).

3.4 Near-field forces

The forces due to near-field (electromagnetic) interactions with other particles are given by

$$\boldsymbol{f}_i^{nf} = \sum_{j=1, j\neq i}^{N_P} \boldsymbol{f}_{ij}^{nf} \,, \tag{9}$$

where $\boldsymbol{f}_{ij}^{nf}$ is the near-field force that acts on particle i due to particle j. This force has the general expression

$$\boldsymbol{f}_{ij}^{nf} = \kappa_1 \left\| \boldsymbol{x}_i - \boldsymbol{x}_j \right\|^{-\lambda_1} \boldsymbol{n}_{ij} - \kappa_2 \left\| \boldsymbol{x}_i - \boldsymbol{x}_j \right\|^{-\lambda_2} \boldsymbol{n}_{ij} \,, \tag{10}$$

in which the κ´s and λ´s are scalar parameters dictating the intensity of the force for the pair $\{i, j\}$ and $\boldsymbol{n}_{ij}$ is the unit vector that points from the center of particle i to the center of particle j, i.e.,

$$\boldsymbol{n}_{ij} = \frac{\boldsymbol{x}_j - \boldsymbol{x}_i}{\left\| \boldsymbol{x}_j - \boldsymbol{x}_i \right\|} \,. \tag{11}$$

This vector will be referred to as the pair´s central direction from now on. In equation (10), scalars κ_1 and λ_1 are related to the attractive part of the force, whereas κ_2 and λ_2 to the repulsive part. This expression may be understood as derived from a generalized Mie´s potential (force potential for atomic and molecular interactions), of which the classical Lennard-Jones potential (see Lennard-Jonnes (1924)) is a special case. It can be used to model e.g. van de Waals effects, pair-wise electrostatic interactions, etc.

3.5 Contact forces

The forces due to contacts or collisions with other particles and/or objects are described here with an overlap-based scheme (also usually called a soft-sphere model). Accordingly, they are a function of the amount of overlap (or local deformation at the contact point) between the contacting pair. We follow Hertz´s elastic contact theory (see e.g. Johnson (1985)) and adopt the following expression for $\boldsymbol{f}_i^{con}$:

$$\begin{aligned} \boldsymbol{f}_i^{con} &= \sum_{j=1}^{N_i^{con}} \boldsymbol{f}_{ij}^{con} \,, \quad \text{with} \\ \boldsymbol{f}_{ij}^{con} &= -\frac{4}{3} \sqrt{r^*} E^* \delta_{ij}^{3/2} \boldsymbol{n}_{ij} - d^{con} \dot{\delta}_{ij} \boldsymbol{n}_{ij} \,, \end{aligned} \tag{12}$$

where N_i^{con} is the number of particles and/or objects that are in contact with particle i, $\boldsymbol{f}_{ij}^{con}$ is the contact force that acts on particle i due to particle or object j,

$$r^* = \frac{r_i r_j}{r_i + r_j} \quad \text{and} \quad E^* = \frac{E_i E_j}{E_j(1-\nu_i^2) + E_i(1-\nu_j^2)} \tag{13}$$

are the effective radius and the effective elasticity modulus of the contacting pair (in which E_i, E_j and ν_i, ν_j are the elasticity modulus and the Poisson coefficient of i and j, respectively), and δ_{ij} is the overlap between the pair, given by

$$\delta_{ij} = r_i + r_j - \left\| \boldsymbol{x}_i - \boldsymbol{x}_j \right\|. \tag{14}$$

Still in equation (12), $\dot{\delta}_{ij}$ is the overlap velocity between the pair (given by the relative velocity between the pair in the pair´s central direction), and

$$d^{con} = 2\xi^{con} \sqrt{2E^* m^* \sqrt{r^*}} \delta_{ij}^{1/4} \tag{15}$$

is a damping constant that is introduced to allow for energy dissipation in the pair´s central direction. This constant is taken here following the ideas of Wellmann and Wriggers (2012), wherein ξ^{con} is the damping rate of the contact or collision (which must be specified) and m^*

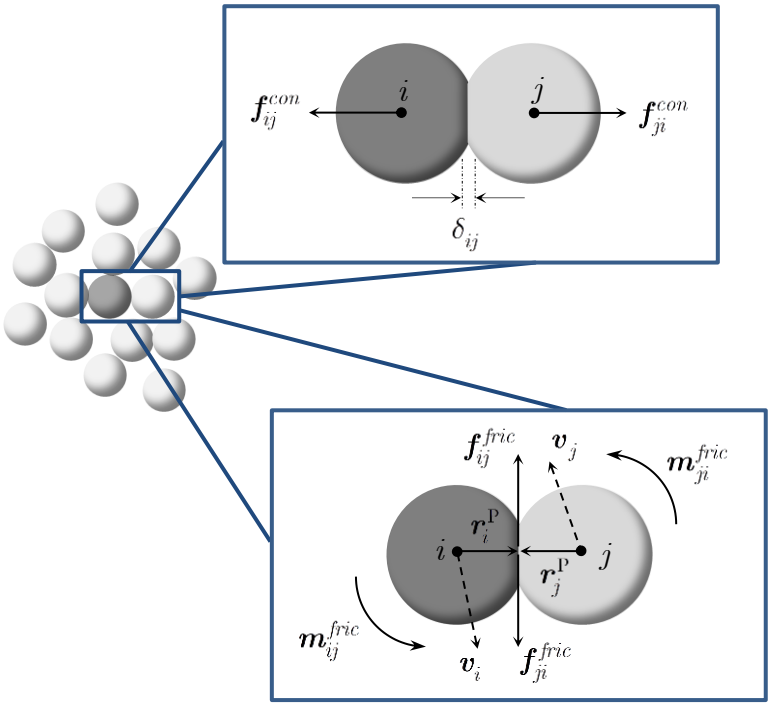

Fig. 2 Contact/collision between two particles

is the effective mass of the contacting pair, i.e.,

$$m^* = \frac{m_i m_j}{m_i + m_j} \,. \tag{16}$$

The value of ξ^{con} may be related to an equivalent coefficient of restitution e (a simplified way is through $\xi^{con} = -\ln e \,/\, (\pi^2 + \ln^2 e)^{1/2}$, which is derived by assuming constant stiffness and constant damping throughout the collision, leading to a velocity-independent e – this is arguable but commonly adopted). We refer the interested reader to Pöschel and Schwager (2004) for several possibilities and a thorough discussion on the subject. Fig. 2 (top part) provides a schematic illustration of the contact/collision for a contacting pair.

3.6 Friction forces

The forces due to friction (which arise from the contacts/collisions) are given by

$$\boldsymbol{f}_i^{fric} = \sum_{j=1}^{N_i^{con}} \boldsymbol{f}_{ij}^{fric} \,, \tag{17}$$

where $\boldsymbol{f}_{ij}^{fric}$ is the friction force that acts on particle i due to particle j. This force is applied at the contact point P on the surface of particle i (see Fig. 2, bottom part), and is modeled here by assuming that sliding and rolling may occur between the contacting pair (whether it is pure sliding, sliding with rolling or pure rolling depends on the motion and the properties of the pair). To describe such phenomena, we devise a scheme based on a tangential spring-dashpot device placed at the contact point in the contact´s tangential direction. Consistent with stick-slip friction models, first we assume that sticking is to occur between the contact

points of the contacting pair. The friction force that will cause such sticking is then applied gradually by the spring-dashpot system, being called a *trial* friction force, with the condition that the static friction limit is not violated. In case a violation is observed, sliding is to occur and thereby the friction force is the dynamic friction. The model reads as follows:

$$\boldsymbol{f}_{ij}^{fric,\mathrm{trial}} = -k^{fric}\Delta\boldsymbol{x}_{ij}^{\mathrm{trial}} - d^{fric}\boldsymbol{v}_{ij}\,, \tag{18}$$

where k^{fric} is the stiffness of the spring, d^{fric} is the damping constant of the dashpot, $\Delta\boldsymbol{x}_{ij}^{\mathrm{trial}}$ is the trial elongation of the spring, and $\boldsymbol{v}_{ij}$ is the elongation velocity. The trial elongation is given by

$$\Delta\boldsymbol{x}_{ij}^{\mathrm{trial}} = \Delta\boldsymbol{x}_{ij}^{\mathrm{accum}} + \delta\boldsymbol{x}_{ij}^{\mathrm{trial}}\,, \tag{19}$$

where $\Delta\boldsymbol{x}_{ij}^{\mathrm{accum}}$ is the accumulated elongation until then (i.e., total elongation acquired in previous configurations, which must be stored) and $\delta\boldsymbol{x}_{ij}^{\mathrm{trial}}$ is the trial *incremental* elongation, i.e., is the trial increase in the elongation observed from the previous to the current configuration only, whose expression will be shown shortly below. The elongation velocity is taken as the relative velocity of the contact points of i and j in the tangential direction, i.e.,

$$\boldsymbol{v}_{ij} = \boldsymbol{v}_{rel,t}^{\mathrm{P}} = \boldsymbol{v}_{rel}^{\mathrm{P}} - (\boldsymbol{v}_{rel}^{\mathrm{P}}\cdot\boldsymbol{n}_{ij})\boldsymbol{n}_{ij}\,, \tag{20}$$

where

$$\boldsymbol{v}_{rel}^{\mathrm{P}} = \boldsymbol{v}_{i}^{\mathrm{P}} - \boldsymbol{v}_{j}^{\mathrm{P}} \tag{21}$$

and, in turn,

$$\boldsymbol{v}_{i}^{\mathrm{P}} = \boldsymbol{v}_{i} + \boldsymbol{\omega}_{i}\times\boldsymbol{r}_{i}^{\mathrm{P}} \quad \text{and} \quad \boldsymbol{v}_{j}^{\mathrm{P}} = \boldsymbol{v}_{j} + \boldsymbol{\omega}_{j}\times\boldsymbol{r}_{j}^{\mathrm{P}}\,. \tag{22}$$

The direction of the trial friction force, denoted by $\boldsymbol{t}_{ij}^{\mathrm{trial}}$, is given by

$$\boldsymbol{t}_{ij}^{\mathrm{trial}} = \frac{\boldsymbol{f}_{ij}^{fric,\mathrm{trial}}}{\left\|\boldsymbol{f}_{ij}^{fric,\mathrm{trial}}\right\|}. \tag{23}$$

In order to verify whether the sticking assumption is valid or not, we define a sliding criterion function F, given by

$$F(\boldsymbol{f}_{ij}^{fric}) = \left\|\boldsymbol{f}_{ij}^{fric}\right\| - \mu_S\left\|\boldsymbol{f}_{ij}^{con}\right\|, \tag{24}$$

such that

$$\begin{cases} F(\boldsymbol{f}_{ij}^{fric,\mathrm{trial}}) \le 0 \Rightarrow \text{the assumption is valid (sticking occurs);} \\ F(\boldsymbol{f}_{ij}^{fric,\mathrm{trial}}) > 0 \Rightarrow \text{the assumption is not valid (sliding occurs).} \end{cases} \tag{25}$$

In (24), μ_S is the static friction coefficient. If the assumption is valid, then $\boldsymbol{f}_{ij}^{fric} = \boldsymbol{f}_{ij}^{fric,\mathrm{trial}}$, $\Delta\boldsymbol{x}_{ij} = \Delta\boldsymbol{x}_{ij}^{\mathrm{trial}}$ and $\boldsymbol{t}_{ij} = \boldsymbol{t}_{ij}^{\mathrm{trial}}$; otherwise, $\boldsymbol{f}_{ij}^{fric} = \mu_D\left\|\boldsymbol{f}_{ij}^{con}\right\|\boldsymbol{t}_{ij}$, wherein μ_D is the dynamic friction coefficient and $\boldsymbol{t}_{ij} = \boldsymbol{t}_{ij}^{\mathrm{trial}}$ is the sliding direction, which is equal to the direction of the trial friction force. In the latter case, the elongation of the spring is not the trial elongation. It must be obtained from equilibrium considerations on the spring-dashpot device: the sliding force must equal the total force on the spring-dashpot, which allows us to write:

$$\mu_D \|\boldsymbol{f}_{ij}^{con}\| \boldsymbol{t}_{ij} = k^{fric} \Delta \boldsymbol{x}_{ij} + d^{fric} \boldsymbol{v}_{ij} \quad \Rightarrow \quad \Delta \boldsymbol{x}_{ij} = \frac{1}{k^{fric}} \; \mu_D \|\boldsymbol{f}_{ij}^{con}\| \boldsymbol{t}_{ij} - d^{fric} \boldsymbol{v}_{ij} \; . \tag{26}$$

This is analogous to the return mapping schemes of plasticity models. At the end, the elongation experienced by the spring must be stored as follows

$$\Delta \boldsymbol{x}_{ij}^{\text{accum}} \leftarrow \Delta \boldsymbol{x}_{ij} \, , \tag{27}$$

such that it may be available for computations of subsequent configurations of the system. Additionally, in order to account for the rotation of the tangent contact plane between two successive configurations, the accumulated elongation must be projected onto the current tangent plane as below

$$\Delta \boldsymbol{x}_{ij}^{\text{accum}} \leftarrow \Delta \boldsymbol{x}_{ij}^{\text{accum}} - (\Delta \boldsymbol{x}_{ij}^{\text{accum}} \cdot \boldsymbol{n}_{ij}) \boldsymbol{n}_{ij} \, . \tag{28}$$

The only missing quantity in this model is the trial incremental elongation $\delta \boldsymbol{x}_{ij}^{\text{trial}}$ of equation (19). This is given here by

$$\delta \boldsymbol{x}_{ij}^{\text{trial}} = \int_{t_{pr}}^{t} \boldsymbol{v}_{rel,t}^{\text{P}}(\tau) d\tau \, , \tag{29}$$

where t_{pr} is the time instant of the previous configuration at which the accumulated elongation $\Delta \boldsymbol{x}_{ij}^{\text{accum}}$ is known, and t is the time at the current configuration. The integration above is computed here as follows

$$\delta \boldsymbol{x}_{ij}^{\text{trial}} \cong \Big[(1-\varphi) \boldsymbol{v}_{rel,t}^{\text{P}}(t_{pr}) + \varphi \boldsymbol{v}_{rel,t}^{\text{P}}(t) \Big] (t - t_{pr}), \quad 0 \leq \varphi \leq 1. \tag{30}$$

The stiffness of the tangential spring is taken here following Mindlin´s solution for elastic tangential deformation of contacting spheres, such that

$$k^{fric} = 8 G^* \sqrt{r^*} \delta_{ij}^{1/2} , \quad \text{with} \quad G^* = \frac{G_i G_j}{G_i + G_j} \tag{31}$$

(G^* is the effective shear modulus of the contacting pair), whereas the damping constant of the dashpot is

$$d^{fric} = 2 \xi^{fric} \sqrt{m^* k^{fric}} \, , \tag{32}$$

with ξ^{fric} as the damping rate. More details can be found in Campello (2016) and Campello (2017).

3.7 Adhesion forces (upon contact)

Adhesion forces may arise only if the particle is in contact with other particles or objects. In such case, the proper consideration of adhesion requires a slight change in the normal contact force of Section 3.5. Accordingly, equation $(12)_2$ needs to be replaced by the following expression:

$$\boldsymbol{f}_{ij}^{con} = \boldsymbol{f}_{ij}^{con,el} + \boldsymbol{f}_{ij}^{adh} + \boldsymbol{f}_{ij}^{con,visc} \, , \tag{33}$$

where $\boldsymbol{f}_{ij}^{con,el}$ is the elastic (repulsive) part of the contact force, $\boldsymbol{f}_{ij}^{adh}$ is the adhesion

(attractive) part of the contact force, and $\boldsymbol{f}_{ij}^{con,visc}$ is the viscous part, which accounts for energy dissipation in the pair´s central direction. The elastic part is given by

$$\boldsymbol{f}_{ij}^{con,el} = -\frac{4}{3}\sqrt{r^*}E^*\delta_{ij}^{3/2}\boldsymbol{n}_{ij} \,, \tag{34}$$

which is the first term of expression $(12)_2$, obtained from Hertz contact theory. The adhesion part, in turn, is derived from JKR´s adhesion theory (see Johnson et al. (1971)), and is given by

$$\boldsymbol{f}_{ij}^{adh} = 2r^{*3/4}\sqrt{2\pi W_{adh}E^*}\delta_{ij}^{3/4}\boldsymbol{n}_{ij} \,, \tag{35}$$

where W_{adh} is the so-called work of adhesion under a fluid, or the free energy change needed to separate a unit contact area of the contacting pair in a fluid medium. This parameter is given by the difference of the respective interfacial surface energies between the particles with themselves and the particles with the fluid (see, e.g., Loskofsky et al. (2006)). The viscous part, in turn, is given by

$$\boldsymbol{f}_{ij}^{con,visc} = -d^{con}\dot{\delta}_{ij}\boldsymbol{n}_{ij} \,, \tag{36}$$

which is identical to the second term of equation $(12)_2$ except for the damping constant, which now reads

$$d^{con} = 2\xi^{con}\sqrt{m^*k_{net}} \,, \tag{37}$$

wherein

$$k_{net} = k_{Hertz} - k_{JKR} = \frac{\partial}{\partial\delta_{ij}}(\boldsymbol{f}_{ij}^{con,el} - \boldsymbol{f}_{ij}^{adh}) = 2E^*\sqrt{r^*\delta_{ij}} - 3r^{*3/4}\sqrt{\frac{1}{2}\pi W_{adh}E^*}\delta_{ij}^{-1/4} \tag{38}$$

is the net stiffness of the normal contact force. This model may be understood as a generalized JKR model.

3.8 Friction moment

The moment generated by the friction forces on particle i (relatively to the center of the particle) is given by

$$\boldsymbol{m}_i^{fric} = \sum_{j=1}^{N_i^{con}} \boldsymbol{r}_i^{\mathrm{P}} \times \boldsymbol{f}_{ij}^{fric}, \tag{39}$$

where we recall that $\boldsymbol{r}_i^{\mathrm{P}}$ is the vector that connects the center of particle i to the contacting point P with particle j (see Fig. 2, bottom part).

3.9 Rolling resistance moment

Rolling resistance is a side effect of the deformation experienced by a particle when it rolls over another particle or object. This deformation, though usually very small, displaces the line of action of the contact force between the contacting pair slightly towards the rolling

direction, implying that a small eccentricity turns to exist in the contact force w.r.t. the pair´s central direction. A moment is thereby generated and, since it is opposed to the rolling rotation, it is called a *rolling resistance* moment. This moment is extremely important in the modeling of particle systems wherein static (or pseud-static) configurations are relevant, such as (but not limited to) piles of grains and compact granular assemblies. We write the total rolling resistance moment acting on a particle as

$$\boldsymbol{m}_i^{rol} = \sum_{j=1}^{N_i^{con}} \boldsymbol{m}_{ij}^{rol}, \tag{40}$$

where $\boldsymbol{m}_{ij}^{rol}$ is the rolling resistance moment acting on particle i due to its rolling over particle (or objetct) j. This, in turn, is described here by following a simple rotational damper model (see e.g. Ai et al. (2011)), such that

$$\boldsymbol{m}_{ij}^{rol} = -\mu_R r^* \left\| \boldsymbol{f}_{ij}^{con} \right\| \frac{\boldsymbol{\omega}_i - \boldsymbol{\omega}_j}{\left\| \boldsymbol{\omega}_i - \boldsymbol{\omega}_j \right\|}, \tag{41}$$

where μ_R is the rolling resistance coefficient for the contacting pair. More elaborate models, such as a rotational spring-dashpot model with a yield moment, are also possible, but not used in this work. This latter model falls in the class of the so-called "elastic-plastic spring-damper" models, as nicely proposed by Ai et al. (2011), and has been widely used by the author as well, with very good results. See Campello (2017) for more details.

Remark. The interactions between particles and objects may be represented as a special case of that between particles. In this sense, objects may be treated as rigid bodies with infinite mass and inertia, the geometry of which being described by a parametric equation that defines its exterior surface (or a set of equations, for the case of multi-facet objects). By doing $r_j \to \infty$, $j_j \to \infty$, $E_j \to \infty$ and $G_j \to \infty$, and using the parametric equation(s) to compute the central direction $\boldsymbol{n}_{ij}$, all expressions above for the forces and moments may be used. For the common case where the objects are flat rigid walls, only a normal vector and a point location in space are needed for their full representation.

3 TIME INTEGRATION SCHEME

Our scheme for solution of the system´s dynamics starts by performing time integration of equation (2) between time instants t and $t + \Delta t$, which furnishes

$$\begin{aligned} \boldsymbol{v}_i(t+\Delta t) &= \boldsymbol{v}_i(t) + \frac{1}{m_i}\int_t^{t+\Delta t} \boldsymbol{f}_i^{tot} dt\,, \\ \boldsymbol{\omega}_i(t+\Delta t) &= \boldsymbol{\omega}_i(t) + \frac{1}{j_i}\int_t^{t+\Delta t} \boldsymbol{m}_i^{tot} dt\,. \end{aligned} \tag{42}$$

The integrals on the right-hand side of (42) are then approximated by using a generalized trapezoidal rule:

$$\begin{aligned}\int_t^{t+\Delta t} \boldsymbol{f}_i^{tot} dt &\approx \Big[\phi \boldsymbol{f}_i^{tot}(t+\Delta t) + (1-\phi)\boldsymbol{f}_i^{tot}(t)\Big]\Delta t\,,\\ \int_t^{t+\Delta t} \boldsymbol{m}_i^{tot} dt &\approx \Big[\phi \boldsymbol{m}_i^{tot}(t+\Delta t) + (1-\phi)\boldsymbol{m}_i^{tot}(t)\Big]\Delta t\,,\end{aligned} \tag{43}$$

in which $0 \leq \phi \leq 1$. When $\phi = 0$, the integration amounts to an (explicit) forward Euler scheme; when $\phi = 1$, to an (implicit) backward Euler one; and when $\phi = 0.5$, to an (implicit) classical trapezoidal rule. By inserting (43) into (42), we have

$$\begin{aligned}\boldsymbol{v}_i(t+\Delta t) &= \boldsymbol{v}_i(t) + \frac{\Delta t}{m_i}\Big[\phi \boldsymbol{f}_i^{tot}(t+\Delta t) + (1-\phi)\boldsymbol{f}_i^{tot}(t)\Big],\\ \boldsymbol{\omega}_i(t+\Delta t) &= \boldsymbol{\omega}_i(t) + \frac{\Delta t}{j_i}\Big[\phi \boldsymbol{m}_i^{tot}(t+\Delta t) + (1-\phi)\boldsymbol{m}_i^{tot}(t)\Big].\end{aligned} \tag{44}$$

On the other hand, by time integration of the velocity and incremental rotation vectors between t and $t+\Delta t$ we have

$$\begin{aligned}\boldsymbol{x}_i(t+\Delta t) &= \boldsymbol{x}_i(t) + \int_t^{t+\Delta t} \boldsymbol{v}_i dt\,,\\ \boldsymbol{\alpha}_i^{\Delta}(t+\Delta t) &= \int_t^{t+\Delta t} \boldsymbol{\omega}_i dt\,.\end{aligned} \tag{45}$$

The generalized trapezoidal rule is then invoked again to approximate the integrals on the right-hand side of (45), rendering

$$\begin{aligned}\int_t^{t+\Delta t} \boldsymbol{v}_i dt &\approx \Big[\phi \boldsymbol{v}_i(t+\Delta t) + (1-\phi)\boldsymbol{v}_i(t)\Big]\Delta t\,,\\ \int_t^{t+\Delta t} \boldsymbol{\omega}_i dt &\approx \Big[\phi \boldsymbol{\omega}_i(t+\Delta t) + (1-\phi)\boldsymbol{\omega}_i(t)\Big]\Delta t\,.\end{aligned} \tag{46}$$

By introducing (46) into (45), we arrive at

$$\begin{aligned}\boldsymbol{x}_i(t+\Delta t) &= \boldsymbol{x}_i(t) + \Big[\phi \boldsymbol{v}_i(t+\Delta t) + (1-\phi)\boldsymbol{v}_i(t)\Big]\Delta t\,,\\ \boldsymbol{\alpha}_i^{\Delta}(t+\Delta t) &= \Big[\phi \boldsymbol{\omega}_i(t+\Delta t) + (1-\phi)\boldsymbol{\omega}_i(t)\Big]\Delta t\,.\end{aligned} \tag{47}$$

Expressions (44) and (47) constitute a set of equations for $i = 1,...,N_P$ particles, with which the velocity, spin, position and incremental rotation vectors of each particle at $t+\Delta t$ may be computed once $\boldsymbol{v}_i(t)$, $\boldsymbol{\omega}_i(t)$ and $\boldsymbol{x}_i(t)$ are known. This computation, however, cannot be performed directly, since (44) requires the evaluation of $\boldsymbol{f}_i^{tot}(t+\Delta t)$ and $\boldsymbol{m}_i^{tot}(t+\Delta t)$, which in turn are functions of all unknown position, velocity, spin and incremental rotation vectors at $t+\Delta t$, i.e.,

$$\begin{aligned}\boldsymbol{f}_i^{tot}(t+\Delta t) &= \hat{\boldsymbol{f}}_i^{tot}\ \ \boldsymbol{x}_j(t+\Delta t), \boldsymbol{v}_j(t+\Delta t), \boldsymbol{\omega}_j(t+\Delta t), \boldsymbol{\alpha}_j^{\Delta}(t+\Delta t)\ \ ,\\ \boldsymbol{m}_i^{tot}(t+\Delta t) &= \hat{\boldsymbol{m}}_i^{tot}\ \ \boldsymbol{x}_j(t+\Delta t), \boldsymbol{v}_j(t+\Delta t), \boldsymbol{\omega}_j(t+\Delta t), \boldsymbol{\alpha}_j^{\Delta}(t+\Delta t)\ \ ,\end{aligned} \tag{48}$$

wherein $j = 1,2,...,N_P$ (the notation with a superposed hat above has been introduced to indicate that the quantity is a function of the arguments inside the parentheses). This means that all equations are strongly coupled and a recursive solution strategy is thereby necessary. We adopt here a fixed-point iterative scheme, following the ideas that have been proposed by Campello and Zohdi (2014a, 2014b) for irrotational particles (i.e. particles without rotational DOFs). The main steps are as summarized in Algorithm 1 below. The scheme is relatively easy to be implemented and it is noteworthy that no system matrix is required.

Algorithm 1. Time integration scheme for solution of the system´s dynamics

1. Known (given) quantities:
   $t = 0$, $\Delta t =$ known, $\phi =$ known, $\boldsymbol{x}_i(t)$, $\boldsymbol{\alpha}_i(t)$, $\boldsymbol{v}_i(t)$, $\boldsymbol{\omega}_i(t) =$ known
2. Initialize time step:
   $K = 0$ (iteration counter)
   $\boldsymbol{x}_i^K(t+\Delta t) = \boldsymbol{x}_i(t)$, $\boldsymbol{\alpha}_j^{\Delta,K}(t+\Delta t) = \boldsymbol{o}$,
   $\boldsymbol{v}_i^K(t+\Delta t) = \boldsymbol{v}_i(t)$, $\boldsymbol{\omega}_i^K(t+\Delta t) = \boldsymbol{\omega}_i(t)$ (predictor)
3. Loop over particles: FOR $i = 1,\ldots,N_P$ DO
   i. Compute force and moment vectors at $t+\Delta t$:
   $$\boldsymbol{f}_i^{tot,K+1}(t+\Delta t) = \hat{\boldsymbol{f}}_i^{tot} \quad \boldsymbol{x}_j^K(t+\Delta t), \boldsymbol{v}_j^K(t+\Delta t), \boldsymbol{\omega}_j^K(t+\Delta t), \boldsymbol{\alpha}_j^{\Delta,K}(t+\Delta t)$$
   $$\boldsymbol{m}_i^{tot,K+1}(t+\Delta t) = \hat{\boldsymbol{m}}_i^{tot} \quad \boldsymbol{x}_j^K(t+\Delta t), \boldsymbol{v}_j^K(t+\Delta t), \boldsymbol{\omega}_j^K(t+\Delta t), \boldsymbol{\alpha}_j^{\Delta,K}(t+\Delta t)$$
   ii. Update velocity and spin vectors:
   $$\boldsymbol{v}_i^{K+1}(t+\Delta t) = \boldsymbol{v}_i(t) + \frac{\Delta t}{m_i}\Big[\phi \boldsymbol{f}_i^{tot,K+1}(t+\Delta t) + (1-\phi)\boldsymbol{f}_i^{tot}(t)\Big]$$
   $$\boldsymbol{\omega}_i^{K+1}(t+\Delta t) = \boldsymbol{\omega}_i(t) + \frac{\Delta t}{j_i}\Big[\phi \boldsymbol{m}_i^{tot,K+1}(t+\Delta t) + (1-\phi)\boldsymbol{m}_i^{tot}(t)\Big]$$
   iii. Update position and incremental rotation vectors
   $$\boldsymbol{x}_i^{K+1}(t+\Delta t) = \boldsymbol{x}_i(t) + \Big[\phi \boldsymbol{v}_i^{K+1}(t+\Delta t) + (1-\phi)\boldsymbol{v}_i(t)\Big]\Delta t$$
   $$\boldsymbol{\alpha}_i^{\Delta,K+1}(t+\Delta t) = \Big[\phi \boldsymbol{\omega}_i^{K+1}(t+\Delta t) + (1-\phi)\boldsymbol{\omega}_i(t)\Big]\Delta t$$
4. Check for convergence
   i. Compute errors $err(\boldsymbol{v})$, $err(\boldsymbol{\omega})$, $err(\boldsymbol{x})$ and $err(\boldsymbol{\alpha}^{\Delta})$
   ii. IF $ANY(error) > TOL \Rightarrow K = K+1$, $GOTO$ (3) (iterate)
   iii. IF $ALL(errors) \leq TOL \Rightarrow t = t + \Delta t$, update $\boldsymbol{\alpha}_i$ and $GOTO$ (2) (next time step)

Finally, after convergence, the total rotation vector of the particles is updated by means of the Rodrigues expression (see Campello (2015) and Campello (2016)):

$$\boldsymbol{\alpha}_i(t+\Delta t) = \frac{4}{4 - \boldsymbol{\alpha}_i(t)\cdot\boldsymbol{\alpha}_i^{\Delta}(t+\Delta t)}\left(\boldsymbol{\alpha}_i(t) + \boldsymbol{\alpha}_i^{\Delta}(t+\Delta t) - \frac{1}{2}\boldsymbol{\alpha}_i(t)\times\boldsymbol{\alpha}_i^{\Delta}(t+\Delta t)\right). \tag{49}$$

Remark. According to what is described in Algorithm 1, one may find that velocities, spins, positions and incremental rotations of all particles are updated only after one complete loop of step (3). This would correspond to a Jacobi-type of scheme and is presented like so only for the sake of algebraic simplicity. What we actually do in step (3) is: for each particle i, we compute $\boldsymbol{f}_i^{tot,K+1}(t+\Delta t)$ and $\boldsymbol{m}_i^{tot,K+1}(t+\Delta t)$ using the velocities, spins, positions and incremental rotations of the particles that have just been updated within the current loop, that is, using $\boldsymbol{v}_j^{K+1}(t+\Delta t)$, $\boldsymbol{\omega}_j^{K+1}(t+\Delta t)$, $\boldsymbol{x}_j^{K+1}(t+\Delta t)$ and $\boldsymbol{\alpha}_j^{\Delta,K+1}(t+\Delta t)$, $j = 1,2,\ldots,i-1$. For $j \geq i$, the values of the previous iteration, i.e., $\boldsymbol{v}_j^K(t+\Delta t)$, $\boldsymbol{\omega}_j^K(t+\Delta t)$, $\boldsymbol{x}_j^K(t+\Delta t)$ and $\boldsymbol{\alpha}_j^{\Delta,K}(t+\Delta t)$, are used. This resembles a Gauss-Seidel scheme, which, as it is well known, converges at a faster rate than the Jacobi method (if the Jacobi method converges) or diverges at a faster rate (if the Jacobi method diverges).

Remark. The error measures in step (4) of the algorithm are taken as normalized (nondimensional) measures, and are given by

$$err(\boldsymbol{a}) = \frac{\sum_{i=1}^{N_p} \left\| \boldsymbol{a}_i^{K+1}(t+\Delta t) - \boldsymbol{a}_i^{K}(t+\Delta t) \right\|}{\sum_{i=1}^{N_p} \left\| \boldsymbol{a}_i^{K+1}(t+\Delta t) - \boldsymbol{a}_i(t) \right\|}, \quad \boldsymbol{a} = \boldsymbol{x}, \boldsymbol{v}, \boldsymbol{\omega} \text{ and } \boldsymbol{\alpha}^{\Delta} . \tag{50}$$

In cases where the denominator in (50) vanishes or approaches zero, we use

$$err(\boldsymbol{a}) = \frac{\sum_{i=1}^{N_p} \left\| \boldsymbol{a}_i^{K+1}(t+\Delta t) - \boldsymbol{a}_i^{K}(t+\Delta t) \right\|}{\sum_{i=1}^{N_p} \left\| \boldsymbol{a}_i^{K+1}(t+\Delta t) \right\|}, \quad \boldsymbol{a} = \boldsymbol{x}, \boldsymbol{v}, \boldsymbol{\omega} \text{ and/or } \boldsymbol{\alpha}^{\Delta}, \tag{51}$$

instead.

4 NUMERICAL EXAMPLES

In this section, we provide three examples of numerical simulations to illustrate how our DEM model may be used to study particle deposition processes. We adopt $\phi = 0.5$ in the time integration scheme throughout (i.e., implicit classical trapezoidal rule in all cases). Selection of the time step size is made according to the duration of a typical contact/collision for the problem at hand. We use the following criterion:

$$\Delta t \leq \frac{\Delta t_{con}}{20}, \quad \text{with} \quad \Delta t_{con} \cong 2.87 \left[\frac{(m^*)^2}{r^* (E^*)^2 v_{rel}} \right]^{1/5}, \tag{52}$$

where Δt_{con} is the duration of a typical contact or collision and v_{rel} is the relative velocity of a typical contacting pair in the pair´s central direction immediately before the contact/collision is initiated. This is based on Hertz´s formula for the duration of elastic collisions and, according to our experience, allows for a good accuracy in the integration of the contact forces. The convergence tolerance used within the iterations (step 4 of Algorithm 1) is $TOL = 10^{-6}$.

4.1 Deposition of a droplet of particles onto an electrified surface

A droplet of charged particles is targeted at an electrified rigid surface, as shown in Fig. 3, top part. The electrification is due to the presence of a uniform electric field of intensity $E = 100$ N/C in the positive x-direction in front of the surface. The particles experience near-field interactions in the form described by equation (10), as well as drag forces (induced by surrounding air) and adhesion forces once in contact (as described by equations (33)-(38)). We want to investigate the behavior of the droplet upon impact with the surface at different incoming velocities. A circle of diameter 50 mm is defined as the target region for deposition at the surface. The droplet is formed by $N_P = 1000$ spherical particles of diameter 1 mm, randomly placed within a fictitious sphere of diameter 40 mm. Its center is positioned 100 mm apart from the front of the surface at time $t = 0$. Other data are as follows:

- mass-density of the particles: $\rho = 1000$ kg/m^3;
- electric charge of the particles: $q = 1$ C;
- elastic properties of the particles: $E = 10^8$ N/m^2 and $\nu = 0$;
- friction coefficients: $\mu_S = \mu_D = 0.1$ (particle-particle) and $\mu_S = \mu_D = 0.4$ (particle-surface);

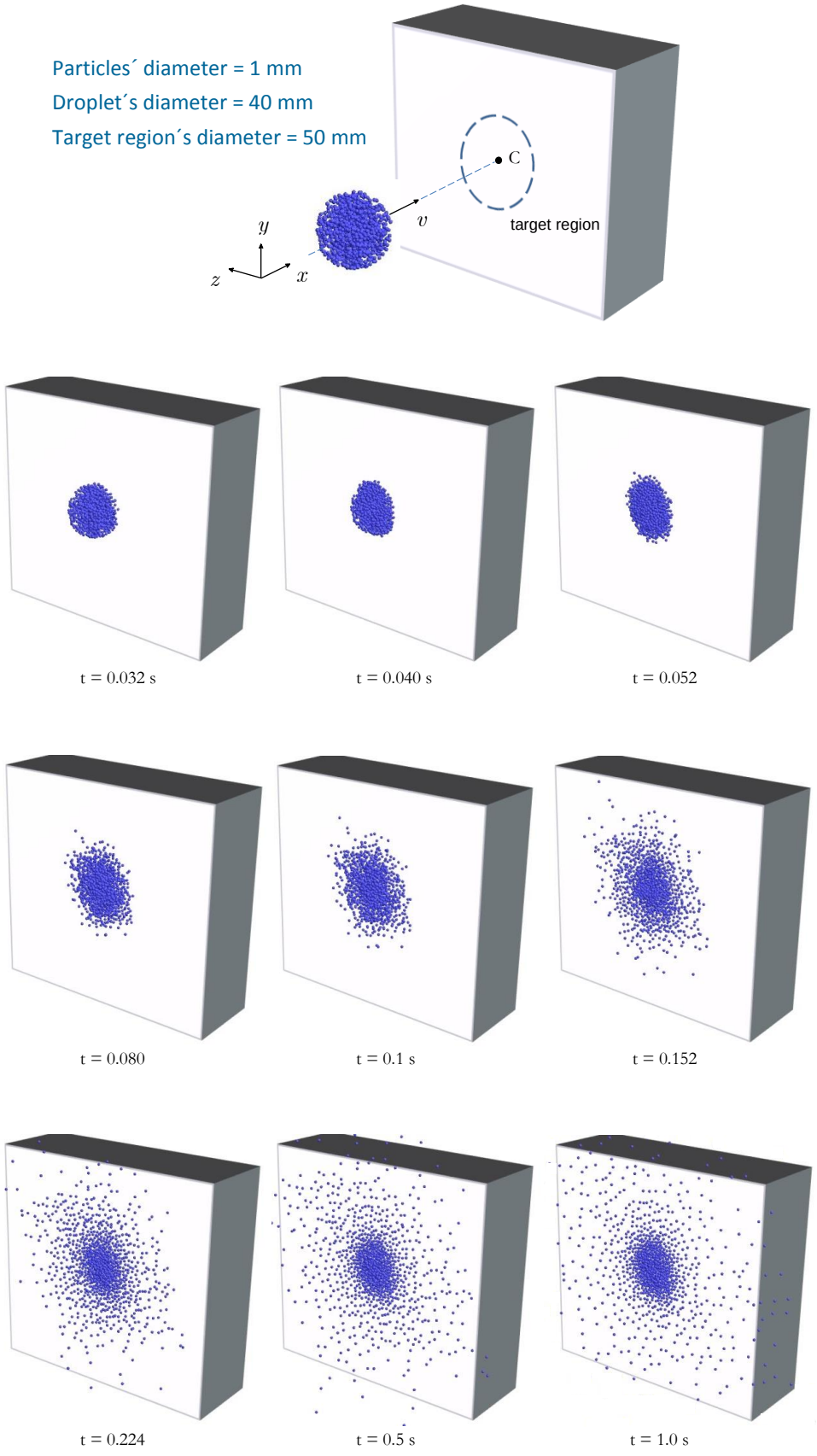

Fig. 3 Deposition of a droplet of particles onto an electrified surface. Problem definition (top) and snapshots of the system´s configuration at selected time instants for a typical simulation (bottom)

- rolling resistance coefficient (particle-particle and particle-surface): $\mu_R = 0.2$;
- damping rates (particle-particle and particle-surface): $\xi^{con} = 0.8$ and $\xi^{fric} = 0.1$;
- near-field forces parameters: $\kappa_1 = 0.5$, $\lambda_1 = 1$, $\kappa_2 = 0.25$ and $\lambda_2 = 2$;
- adhesion forces parameter (work of adhesion): $W_{adh} = 10$ N·m;
- surrounding air´s density and viscosity: $\rho_F = 1.2$ kg/m^3 and $\eta_F = 1.8 \times 10^{-5}$ Pa·s;
- gravity acceleration: $g = -9.81$ m/s^2 (x-direction);
- droplet velocity (x-direction): $v = 1, 5, 10, 20, 25$ and 50 m/s;
- time-step size: $\Delta t = 1 \times 10^{-4}$ s (with step size adaptivity, wherein $\Delta t_{\max} = \Delta t$ and $\Delta t_{\min} = 0.1\Delta t$), with $t_F = 1.0$ s as the time at the end of the simulation.

Figure 3, bottom part, shows snapshots of the system´s configuration at selected time instants for a typical simulation (the case shown is for $v = 20$ m/s and $W_{adh} = 1$ N·m). One can see the dynamics of the droplet upon impact and the evolution of the particles´ motion over the surface. As it can be seen, a reasonable amount of particles does not adhere to each other but instead spread outside the target region, wherein they eventually stop and remain stick to the surface due to the action of the electric field. For the other droplet velocities, the final configurations obtained at $t_F = 1.0$ s are shown in Fig. 4. Table 1 provides the values of the mean distance of the particles to point C (center of the target region), the maximum thickness of the deposited material, and the percentage of material deposited within the target region for each case. Ten simulations were run for each case; results are averaged.

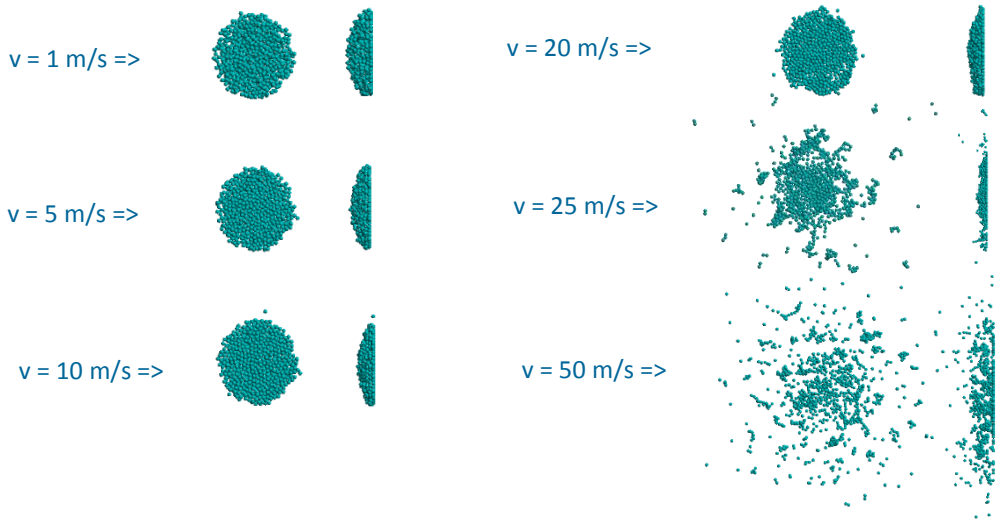

Fig. 4 Deposition of a droplet of particles onto an electrified surface. Final configurations obtained for each droplet velocity (top and side views)

Table 1. Deposition of a droplet of particles onto an electrified surface. Properties of the deposited material.

Droplet velocity	Mean distance to C (and standard deviation)	Maximum thickness of deposited material (and standard deviation)	Percentage of material deposited within target region (and st. dev.)
1 m/s	11.8 mm (1.2 mm)	9.2 mm (0.6 mm)	99.9% (0)
5 m/s	14.4 mm (1.1 mm)	8.1 mm (0.5 mm)	99.9% (0)
10 m/s	15.9 mm (1.1 mm)	6.9 mm (0.5 mm)	99.7% (0.1%)
20 m/s	16.2 mm (1.4 mm)	5.8 mm (0.6 mm)	92.2% (1.4%)
25 m/s	21.2 mm (3.7 mm)	5.5 mm (1.3 mm)	71% (3.1%)
50 m/s	26.2 mm (4.2 mm)	2.2 mm (1.9 mm)	55.1% (6.2%)

4.2 Deposition of a jet of particles onto a rigid surface

A jet of particles is deposited onto a rigid surface with the aim that they adhere and form a protective layer or coating to the surface, as indicated in Fig. 5, top part. We want to investigate what is the appropriate jet velocity v_x such that good adherence and coherence are observed for the deposited material. The jet consists of $N_P = 1500$ spherical particles (placed randomly within a fictitious prism of dimensions 10 cm x 1.5 cm x 1.5 cm), the radii of which follow a Gaussian distribution of mean $\overline{r} = 2.0$ mm and standard deviation $\sigma_r = 0.2$ mm (the distribution is truncated at three standard deviations from the mean such that all radii lie in the interval [1.4 mm, 2.6 mm]). The jet moves in the positive y-direction at a constant speed of 5 m/s. The adhesion of the particles with the surface (and also with themselves) is represented by forces in the form of equations (33)-(38). Drag forces given by equation (6) are also considered (the medium surrounding the particles is dry air). No near-fields effects are present. Other parameters are:

- mass-density of the particles: $\rho = 1000$ kg/m^3;
- elastic properties of the particles: $E = 1 \times 10^7$ N/m^2 and $\nu = 0.25$;
- friction coefficient between particles: $\mu_S = \mu_D = 0.05$;
- friction coefficient between particles and the rigid surface: $\mu_S = \mu_D = 0.4$;
- rolling resistance coefficient between particles: $\mu_R = 0.1$;
- rolling resistance coefficient between particles and the rigid surface: $\mu_R = 0.25$;
- damping rates (particle-particle and particle-rigid surface): $\xi^{con} = 0.8$ and $\xi^{fric} = 0.1$;
- adhesion forces parameter (work of adhesion): $W_{adh} = 10^3$ N·m;
- dry air mass-density and viscosity: $\rho_F = 1.2$ kg/m^3 and $\eta_F = 1.8 \times 10^{-5}$ Pa·s;
- gravity acceleration: $g = -9.81$ m/s^2 (x-direction);
- jet velocity: $v_x = 1,\ 5,\ 10$ and 20 m/s;
- time-step size: $\Delta t = 1 \times 10^{-4}$ s;
- time at the end of the simulation: $t_F = 1.0$ s.

Figure 5, bottom part, shows snapshots of the simulation at selected time instants for each one of the jet velocities considered. As it can be observed, the case with $v_x = 1$ m/s is not able to enforce adherence. For the other cases, however, there is practically complete adherence plus good coherence, though the visual aspect of the deposited layer (after the particles have come to a complete rest) is quite different for each velocity. When $v_x = 5$ m/s, the layer is long, narrow and thin; when $v_x = 10$ m/s, it is less long and a bit wider and thicker than the previous case; and when $v_x = 20$ m/s, it has a very compact aspect, being also thicker. Each one of these characteristics may be more or less desirable, depending on the application one is interested in. Table 2 provides values of the mean thickness, width and length of the layer for each case. Results are averaged over ten simulations for each case.

Table 2. Deposition of a jet of particles onto a rigid surface. Deposited layer properties.

Jet velocity	Mean thickness of deposited layer (and standard deviation)	Mean width (and standard deviation)	Layer length
1 m/s	--	--	--
5 m/s	0.9 cm (0.32 cm)	1.4 cm (0.22 cm)	28 cm (1.0 cm)
10 m/s	1.4 cm (0.61 cm)	1.9 cm (0.42 cm)	13 cm (0.8 cm)
20 m/s	1.6 cm (0.72 cm)	2.4 cm (0.71 cm)	9 cm (0.6 cm)

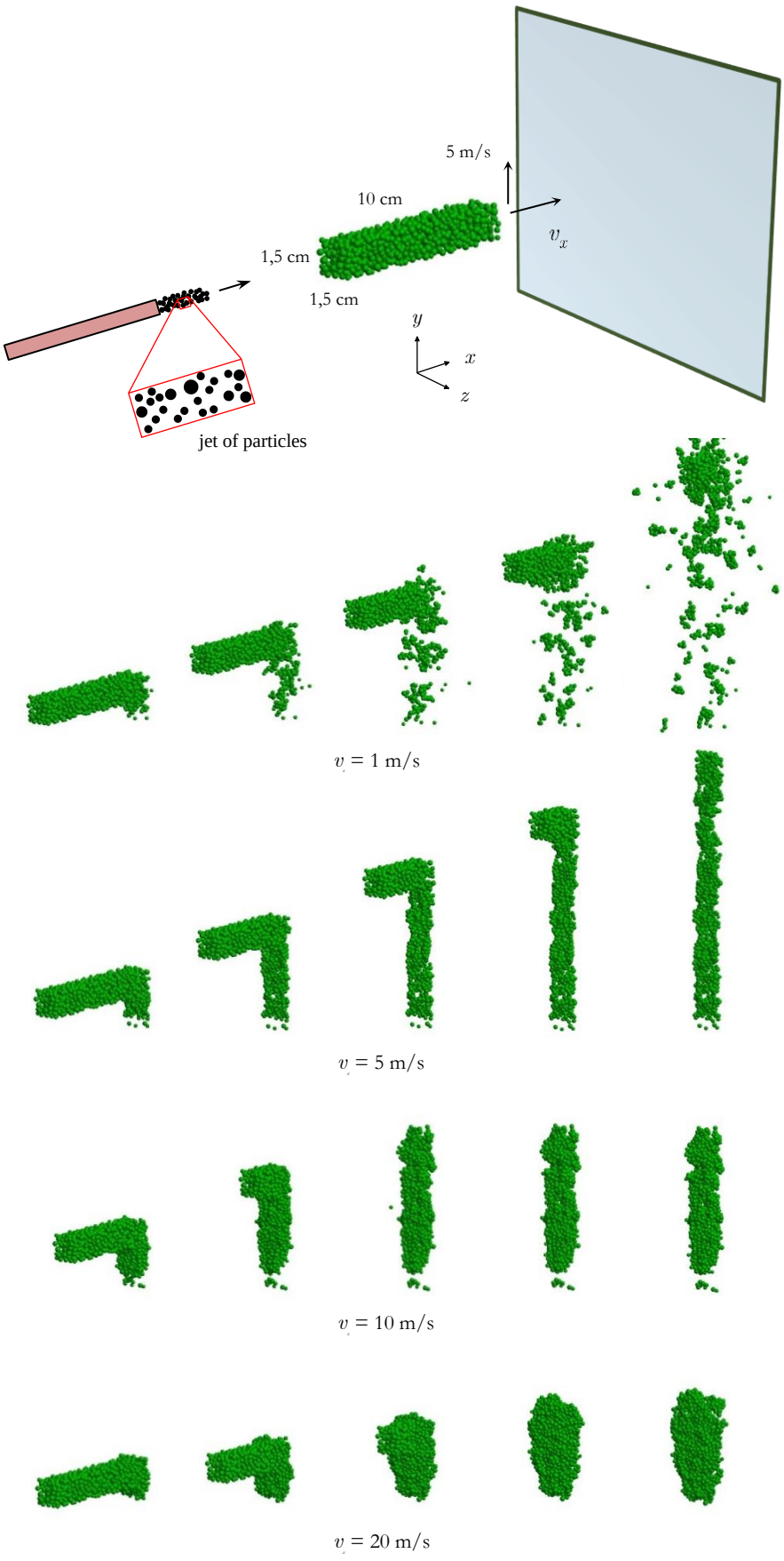

Fig. 5 Deposition of a jet of particles onto a rigid surface. Problem definition (top) and analysis results (bottom)

4.3 3D printing of a U-shape

In this example we simulate the fabrication of a U-shape member from a 3D printer. The printer nozzle moves horizontally over a base platform and jets particles in three successive straight segments (or "legs"), creating a U-shaped layer of material. Once the layer is finished, the nozzle moves backwards in the same path, jetting another layer on top of the previous one. The process is repeated multiple times until a certain desired height is reached (this requires the nozzle to also move up vertically), giving birth to a three-dimensional U-shape member. We consider the deposition material with the same properties as in the previous example (same particle size distribution, same material properties and same contact, friction and rolling resistance parameters), except for the adhesion force parameter, which is taken here as $W_{adh} = 200$ N·m. The particles are jetted at the impact speed of 10 m/s, while the horizontal velocity of the nozzle is 5 m/s. All other data are taken exactly as in the previous example. Figure 6 shows snapshots of the system´s configuration at selected time instants as obtained with our simulation. As it can be seen, the "legs" of the each layer are deposited with reasonable accuracy and very good definition. This is due to the adopted jet velocity (for this set of material parameters). Higher impact velocities lead to a degradation in both accuracy and definition, which becomes progressively stronger with the increase in the jet speed – eventually ending up in a complete spreading of the material over the base platform. Lower impact velocities, on the other side, lead to wider and less sharp layers, also of non-uniform thickness, degrading both the efficiency of the process and the definition of the finished shape.

5 CONCLUSIONS

The main purpose of this work was to present a simple computational model for the simulation of industrial particle deposition processes. Many real applications may be studied with models of such type. Analysts and engineers may, e.g., explore in a relatively rapid and straightforward way the influence of several process parameters on the deposition, thus being able to identify general trends that my eventually help improve the efficiency and quality of the process they are interested in. As future research, which is already being conducted by the author, heat effects will be incorporated into the model, leading to a coupled (thermal-mechanical) system which may be used to study processes wherein particle heating and melting, with phase transformation, occur. These include, e.g., laser sintering methods, which are being more and more favored in the manufacturing industry. The author believes that consistent DEM models may be a useful tool for the simulation of many modern particle deposition processes, such as (but not limited to) additive manufacturing techniques, 3D printing methods, deposition of thermal and mechanical barrier coatings onto surfaces, and many others wherein matter is additively placed into shape.

ACKNOWLEDGEMENTS

This work was supported by CNPq (Conselho Nacional de Desenvolvimento Científico e Tecnológico) and FAPESP (São Paulo State Science Foundation), under the grants 303793/2012-0 and 2014/19821-7, respectively. Support from IUTAM (International Union of Theoretical and Applied Mechanics), and colleague Tarek Zohdi (University of California at Berkeley, USA)) are likewise gratefully acknowledged.

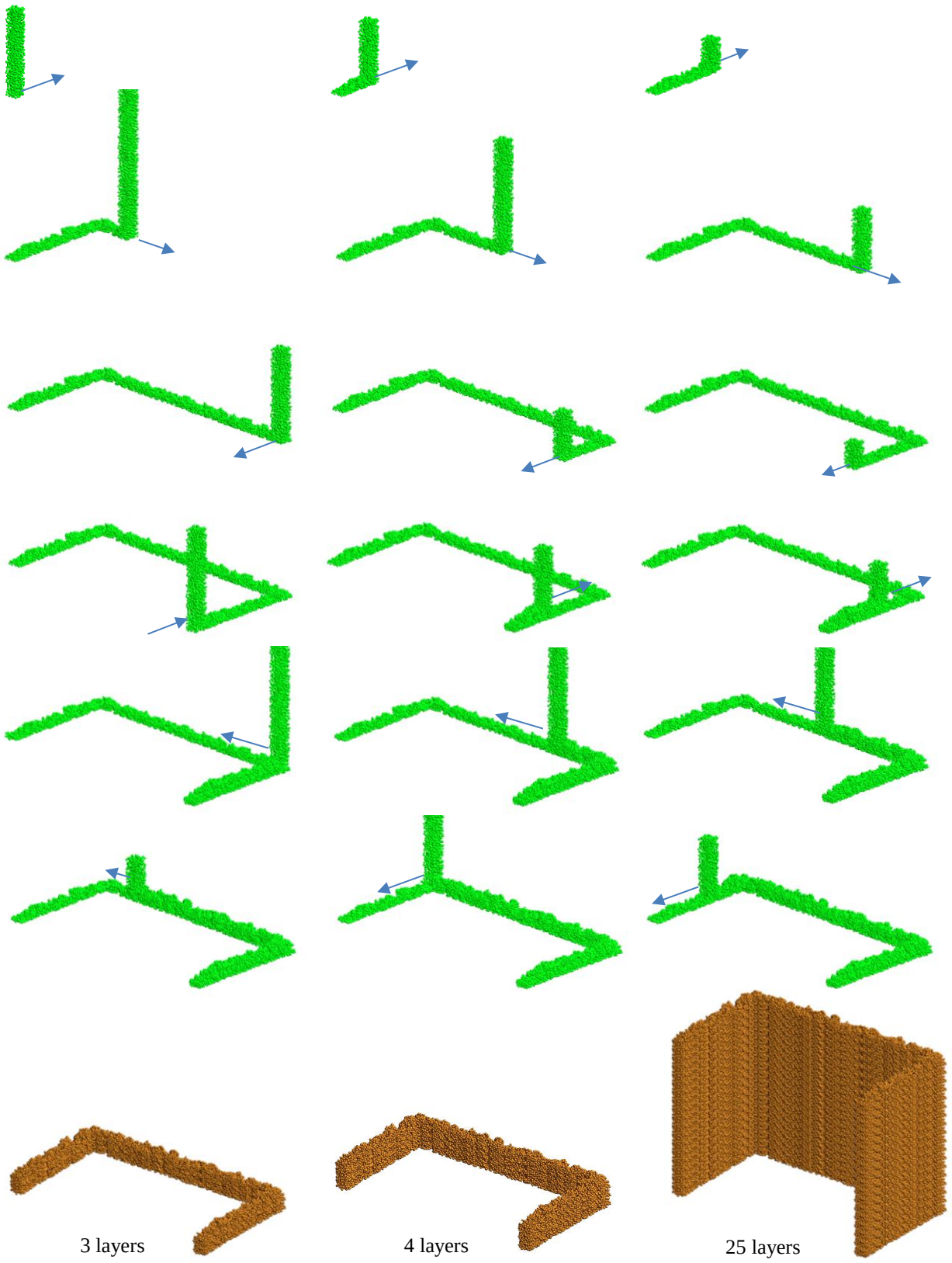

Fig. 6 3D printing of a U-shape. Snapshots of the process. Sequence is from left to right, top to bottom.

REFERENCES

Ai, J., Chen, J.-F., Rotter, J. M., Ooi, J. Y., 2011. Assessment of rolling resistance models in discrete element simulations. Powder Technology 206:269–282.

Biringen, S., Chow, C.-Y., 2011. *An introduction to computational fluid mechanics by example*. Hoboken: Wiley.

Campello, E. M. B., 2017 (submitted). A computational model for the simulation of dry granular materials. *Acta Mechanica*.

Campello, E. M. B., 2016. *Um modelo computacional para o estudo de materiais granulares*. Tese de Livre-Docência, Escola Politécnica da Universidade de São Paulo. 100p.

Campello, E. M. B., 2015a. A description of rotations for DEM models of particle systems. *Computational Particle Mechanics* 2:109–125.

Campello, E. M. B., 2015b. Computational modeling and simulation of rupture of membranes and thin films. *Journal of the Brazilian Society of Mechanical Sciences and Engineering* 37:1793-1809.

Campello, E. M. B., Zohdi, T., 2014a. A computational framework for simulation of the delivery of substances into cells. *International Journal for Numerical Methods in Biomedical Engineering* 30:1132–1152.

Campello, E. M. B., Zohdi, T., 2014b. Design evaluation of a particle bombardment system used to deliver substances into cells. *Computer Modeling in Engineering & Sciences* 98(2):221–245.

Campello, E. M. B., Pimenta, P. M. and Wriggers, P., 2011. An exact conserving algorithm for nonlinear dynamics with rotational dofs and general hyperelasticity. Part2: Shells. *Computational Mechanics* 48:195–211.

Johnson, K. L., 1985. *Contact Mechanics*. Cambridge: Cambridge University Press.

Johnson, K. L., Kendall, K., and Roberts, A. D., 1971. Surface Energy and Contact of Elastic Solids. *Proc. R. Soc. London*, Ser. A, 324, 301–313.

Lennard-Jones, J. E., 1924. On the Determination of Molecular Fields. Proceedings of the Royal Society of London A 106(738): 463–477.

Loskofsky, C., Song, F., and Newby, B. Z., 2006. Underwater Adhesion Measurements Using the JKR Technique. *The Journal of Adhesion* 82:713–730.

Pöschel, T., Schwager, T., 2004. *Computational Granular Dynamics*. Berlin: Springer.

Wellmann, C., Wriggers, P., 2012. A two-scale model of granular materials. *Computer Methods in Applied Mechanics and Engineering* 205–208:46–58.

Zhu, H. P., Zhou, Z. Y., Yang, R. Y., Yu, A. B., 2008. Discrete particle simulation of particulate systems: a review of major applications and findings. *Chemical Engineering Science* 63:5728–5770.

Zohdi, T. I., 2102. *Dynamics of charged particulate systems: Modeling, theory and computation*. New York: Springer.